LETTER

doi:10.1038/nature17973

Molecular mechanism of APC/C activation by mitotic phosphorylation

Suyang Zhang[1]*, Leifu Chang[1]*, Claudio Alfieri[1], Ziguo Zhang[1], Jing Yang[1], Sarah Maslen[1], Mark Skehel[1] & David Barford[1]

In eukaryotes, the anaphase-promoting complex (APC/C, also known as the cyclosome) regulates the ubiquitin-dependent proteolysis of specific cell-cycle proteins to coordinate chromosome segregation in mitosis and entry into the G1 phase[1,2]. The catalytic activity of the APC/C and its ability to specify the destruction of particular proteins at different phases of the cell cycle are controlled by its interaction with two structurally related coactivator subunits, Cdc20 and Cdh1. Coactivators recognize substrate degrons[3], and enhance the affinity of the APC/C for its cognate E2 (refs 4–6). During mitosis, cyclin-dependent kinase (Cdk) and polo-like kinase (Plk) control Cdc20- and Cdh1-mediated activation of the APC/C. Hyperphosphorylation of APC/C subunits, notably Apc1 and Apc3, is required for Cdc20 to activate the APC/C[7–12], whereas phosphorylation of Cdh1 prevents its association with the APC/C[9,13,14]. Since both coactivators associate with the APC/C through their common C-box[15] and Ile-Arg tail motifs[16,17], the mechanism underlying this differential regulation is unclear, as is the role of specific APC/C phosphorylation sites. Here, using cryo-electron microscopy and biochemical analysis, we define the molecular basis of how phosphorylation of human APC/C allows for its control by Cdc20. An auto-inhibitory segment of Apc1 acts as a molecular switch that in apo unphosphorylated APC/C interacts with the C-box binding site and obstructs engagement of Cdc20. Phosphorylation of the auto-inhibitory segment displaces it from the C-box-binding site. Efficient phosphorylation of the auto-inhibitory segment, and thus relief of auto-inhibition, requires the recruitment of Cdk–cyclin in complex with a Cdk regulatory subunit (Cks) to a hyperphosphorylated loop of Apc3. We also find that the small-molecule inhibitor, tosyl-L-arginine methyl ester, preferentially suppresses APC/C^{Cdc20} rather than APC/C^{Cdh1}, and interacts with the binding sites of both the C-box and Ile-Arg tail motifs. Our results reveal the mechanism for the regulation of mitotic APC/C by phosphorylation and provide a rationale for the development of selective inhibitors of this state.

To understand how multi-site phosphorylation of numerous APC/C subunits stimulates the capacity of Cdc20 to control the APC/C we determined a series of APC/C structures in different functional states to near-atomic resolution (Extended Data Table 1a). We used the kinases Cdk2–cyclin A3–Cks2 and Polo (Plk1) to phosphorylate *in vitro* recombinant human APC/C[11,12,18,19] (Extended Data Fig. 1a), obtaining APC/C in the mitotic state that can be activated by Cdc20 (Extended Data Fig. 1b, lanes 9, 10). This reconstituted APC/C recapitulates Cdk- and Plk1-dependent activation of endogenous APC/C^{Cdc20} (refs 8–12). Kinase treatment resulted in a complete upshift of the Apc3 subunit as visualized on SDS–PAGE, indicative of stoichiometric phosphorylation (Extended Data Fig. 1a, c). Almost 150 phosphorylation sites were identified in phospho-APC/C by mass spectrometry (Extended Data Tables 2 and 3), matching published data[12,20–22]. These sites lie within disordered regions of the APC/C[23]. Incubating the APC/C with both Cdk2–cyclin A3–Cks2 and Plk1 simultaneously was necessary to obtain full activation (Extended Data Fig. 1b). Consistent with ref. 12, treatment with Cdk2–cyclin A3–Cks2 alone resulted in lower APC/C activation, whereas phosphorylation with Plk1 alone did not activate the APC/C.

To gain insights into the molecular interactions between Cdc20 and mitotic APC/C, a ternary complex was assembled using phosphorylated APC/C, Cdc20 and a high-affinity substrate Hsl1 (APC/C$^{Cdc20\text{-}Hsl1}$) (Extended Data Fig. 1d) for cryo-EM analysis (Fig. 1a, b, Extended Data Fig. 1e–g and Extended Data Table 1). Owing to the low occupancy of Cdc20 bound to the APC/C, combined with conformational heterogeneity, only 9% of the particles were used for the final reconstruction of APC/C$^{Cdc20\text{-}Hsl1}$, with the remainder being in either the apo state (72%) or in a hybrid state (Extended Data Fig. 2). Most static regions of the complex extend beyond 3.9 Å resolution, whereas the catalytic module (Apc2 and Apc11), as well as the WD40 domain of Cdc20, are more flexible (Extended Data Fig. 3a).

APC/C$^{Cdc20\text{-}Hsl1}$ adopts an active conformation with the catalytic module in the upward position reminiscent of APC/C$^{Cdh1\text{-}Hsl1}$ (ref. 6) (Fig. 1a, b, Extended Data Fig. 4a, b and Supplementary Video 1) and in agreement with a low-resolution negative-stain EM reconstruction of APC/C^{Cdc20} (ref. 24). Relative to Cdh1^{WD40}, the Cdc20^{WD40} domain is shifted away from the APC/C by as much as 10 Å (Extended Data Fig. 3b). Its interaction with the APC/C involves only its N-terminal domain (Cdc20^{NTD}) and the C-terminal Ile–Arg (IR) tail (Cdc20^{IR}) (Fig. 1c–e, Extended Data Figs 3c–e and 4c, d). Compared with Cdh1^{NTD}, Cdc20^{NTD} forms fewer contacts with both Apc1 and Apc8B (Fig. 1c–e). However, the crucial C-box motif (DRYIPxR) represents a structurally conserved region common to both coactivators (Fig. 1d, Extended Data Figs 3c, d and 4d). Cdc20$^{C\,box}$ forms a network of electrostatic interactions with Apc8B, centred on the crucial Arg78 (ref. 23), and augmented by non-polar interactions involving its Tyr79 and Ile80 residues (Fig. 1d). A KILR motif also present within Cdc20^{NTD} is essential for Cdc20 association with the APC/C (ref. 25) and the APC/C$^{Cdc20\text{-}Hsl1}$ structure reveals that Ile130 and Leu131 of Cdc20^{KILR} are inserted into a hydrophobic pocket of the TPR (tetratricopeptide repeat) superhelix of Apc8B, further stabilizing the conformation of the C box (Fig. 1e). Similar C-box stabilization is present in Cdh1^{NTD}, but is instead provided by a loop structurally unrelated to Cdc20^{KILR} (Fig. 1c)[23]. By contrast, the KLLR-motif of Cdh1^{NTD} is located in a leucine-zipper-like α-helix (α3) that forms a hydrophobic interface with Apc1 (ref. 23) (Fig. 1c and Extended Data Fig. 4d). The absence of an equivalent to the Cdh1 α3 helix in Cdc20 suggests a weaker mode of binding of Cdc20^{NTD} relative to Cdh1^{NTD}.

EM density for Cdc20^{IR} is weaker than for Cdh1^{IR} and it lacks the associated α-helix of Cdh1^{IR} (Extended Data Fig. 3e). This could account for the lower affinity of the APC/C for Cdc20^{IR} compared with Cdh1^{IR} (ref. 17). Nonetheless, the crucial Ile–Arg interaction of Cdc20^{IR} with the TPR superhelix of Apc3A is conserved between the two coactivators (Extended Data Fig. 3e). Importantly, because in the APC/C$^{Cdc20\text{-}Hsl1}$ EM structure, densities corresponding to phosphorylated residues

[1]MRC Laboratory of Molecular Biology, Francis Crick Avenue, Cambridge CB2 0QH, UK.
*These authors contributed equally to this work.

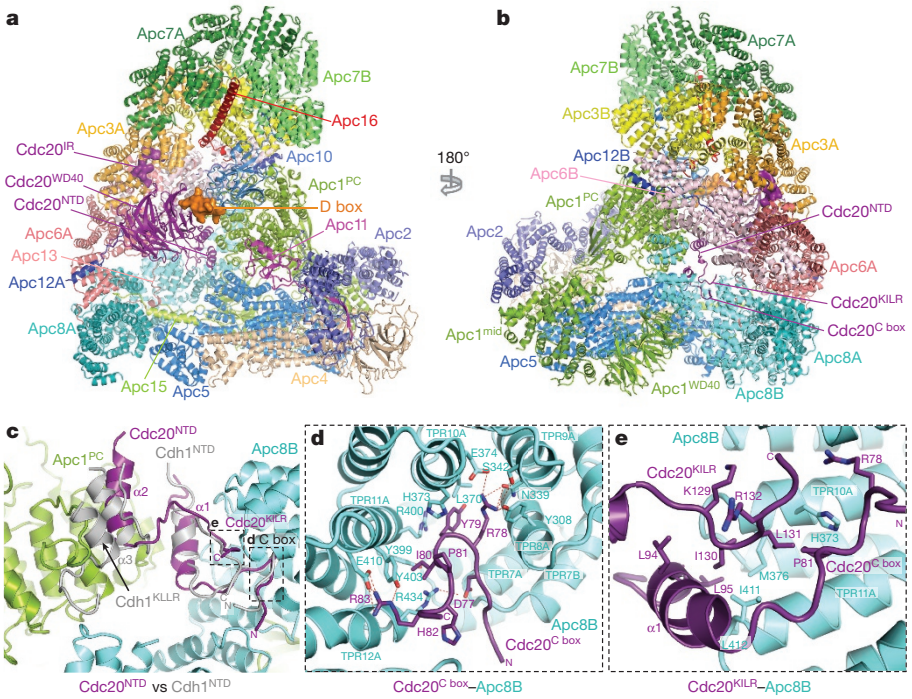

Figure 1 | EM reconstructions of the APC/C$^{Cdc20\text{-}Hsl1}$ complex and comparison of Cdc20^{NTD} and Cdh1^{NTD}. **a**, **b**, Two views of APC/C$^{Cdc20\text{-}Hsl1}$ shown in cartoon with the D-box and Cdc20^{IR} highlighted in surface representation. Cdc20 binds to the APC/C in juxtaposition to Apc10 to form the substrate recognition module. Apc1 is composed of an N-terminal WD40 domain Apc1^{WD40}, a middle domain Apc1^{mid} and a C-terminal Apc1^{PC} domain. Apc11 is modelled based on the APC/C$^{Cdh1\text{-}Emi1}$ structure (PDB 4UI9)[22]. **c**, Both Cdc20^{NTD} (purple) and Cdh1^{NTD} (grey, aligned to APC/C$^{Cdc20\text{-}Hsl1}$)[23] interact with Apc1 and Apc8B, whereas Cdh1^{NTD} contains an additional α3 helix associating with Apc1. **d**, The crucial C-box motif is well conserved between the two coactivators and forms extensive interactions with Apc8B. **e**, The KLLR motif of Cdh1 is present in the α3 helix to engage Apc1, whereas the related Cdc20^{KILR} motif contacts Apc8B to augment C-box binding.

are not visible, we find no evidence that phosphorylated regions of the APC/C either directly or indirectly contact Cdc20. This suggested that APC/C phosphorylation invokes a conformational change of apo APC/C that promotes its association with Cdc20.

To explore this possibility, we determined cryo-EM structures of apo APC/C in both the unphosphorylated and phosphorylated states at near-atomic resolution (Fig. 2a, b, Extended Data Fig. 5a, b, Extended Data Table 1 and Supplementary Video 1). In both states, the catalytic module adopts an inactive conformation (Extended Data Fig. 4a, b) as seen in the previous 8 Å resolution reconstruction[6]. However, three-dimensional classification of the atomic resolution EM maps of both apo states showed that the majority of Apc3A adopts a closed conformation resembling the Apc3 crystal structure in which an α-helix (TPR12A) occupies and blocks the IR tail-binding pocket (Extended Data Fig. 5c)[26]. In ~30% of particles Apc3A adopts an open conformation identical to the IR tail-bound state. Thus inter-conversion of Apc3A between closed and open IR tail-accessible states is not controlled by phosphorylation.

Phosphorylated and unphosphorylated apo APC/C EM maps are very similar in structure (Extended Data Fig. 5a, b), except for a notable difference in the region of the C-box binding site (Fig. 2c–f). In unphosphorylated APC/C, an unassigned segment of EM density of ~15 residues indicative of an elongated loop connected to a short α-helix is located at the C-box binding pocket of Apc8B (Fig. 2c–e). The equivalent EM density is not present in phosphorylated APC/C (Fig. 2f). The WD40 domain of Apc1, positioned in close proximity to this density, incorporates two highly phosphorylated regions (residues 307–395 (300s loop) and residues 515–579 (500s loop)) (Fig. 2c, d and Extended Data Table 2), which have not previously been assigned in either APC/C$^{Cdc20\text{-}Hsl1}$ or APC/C$^{Cdh1\text{-}Emi1}$ structures[23]. The 300s loop would be predicted to project towards the C-box binding site of Apc8B (Fig. 2c, d and Extended Data Fig. 5d), implicating it as a candidate for the unassigned density segment.

We determined the structure of an APC/C mutant with the 300s loop of Apc1 deleted (APC/C$^{\Delta Apc1\text{-}300s}$) (Fig. 2g and Extended Data Table 1a). In this structure, the C-box binding pocket of APC/C$^{\Delta Apc1\text{-}300s}$ is devoid of EM density even without *in vitro* phosphorylation (Fig. 2g), consistent with its assignment to the 300s loop. Furthermore, ubiquitination assays showed that APC/C$^{\Delta Apc1\text{-}300s}$ was constitutively activated by Cdc20 and that phosphorylation did not enhance its activity (Fig. 3a, compare lanes 6, 7 to 8, 9). This indicates that unphosphorylated APC/C is maintained in an auto-inhibited conformation by an Apc1 auto-inhibitory segment, present within the 300s loop that sterically impedes the C-box site from binding Cdc20. In support of this idea, analytical size-exclusion chromatography showed that Cdc20 forms a binary complex with phosphorylated APC/C, but not with unphosphorylated APC/C (Extended Data Fig. 6a), in agreement with refs 10,12.

To identify the auto-inhibitory segment within the Apc1 300s loop, we synthesized a set of eight overlapping peptides of 20 residues, spanning the 300s loop, and tested their potential to inhibit APC/C$^{\Delta Apc1\text{-}300s}$ (Fig. 3b). Notably, peptide 7 (residues 361–380, Fig. 3b, lane 9) potently suppressed Cdc20-dependent APC/C$^{\Delta Apc1\text{-}300s}$ activity. Interestingly, an Arg368–Phe369 pair of this peptide, that resembles the Arg78–Tyr79 of the C box, is flanked by four serine residues phosphorylated in mitotic APC/C (Fig. 3c and Extended Data Table 2)[12,21,22].

EM density for the auto-inhibitory segment is weak, probably due to partial occupancy at the C-box site (Fig. 3c). Nevertheless, side chain density similar to Arg78–Tyr79 of the C box suggests a fit for the Arg–Phe of peptide 7 (Arg368–Phe369) (Fig. 3c). To test the possibility that the Apc1 auto-inhibitory segment corresponds to peptide 7, we synthesized mutants of peptide 7 and also introduced the equivalent mutations into Apc1 of the recombinant APC/C. Replacing Arg368 with Glu in Apc1 resulted in a Cdc20-dependent activation of unphosphorylated APC/C (Fig. 3d), and reduced the inhibitory potency of peptide 7 towards APC/C$^{\Delta Apc1\text{-}300s}$ (Extended Data Fig. 6c). A similar result was obtained on substituting glutamates for the four neighbouring serine residues (Ser364, Ser372, Ser373 and Ser377 (APC/C$^{Apc1\text{-}4S/E}$)) to mimic phosphorylation (Fig. 3d and Extended Data Fig. 6c). Phosphorylation of Ser377 of peptide 7 relieved the inhibition only partially. These findings suggest that Arg368 anchors the Apc1 auto-inhibitory segment to the C-box binding site, mimicking the Cdc20 C box, and maintaining the apo APC/C in an auto-inhibited state. Phosphorylation of the four neighbouring serine residues would destabilize its association with the C-box site (Figs 3c and 4a). This mechanism could be further tested in an *in vivo* context by cellular assays.

Our results so far reveal that the critical determinant of APC/C^{Cdc20} activation by phosphorylation is displacement of the Apc1 auto-inhibitory segment from the C-box site. However, since Apc3 is hyperphosphorylated in mitosis, and Cks stimulates both Cdk-dependent activation of APC/C^{Cdc20} (refs 18,19) and Apc1 and Apc3

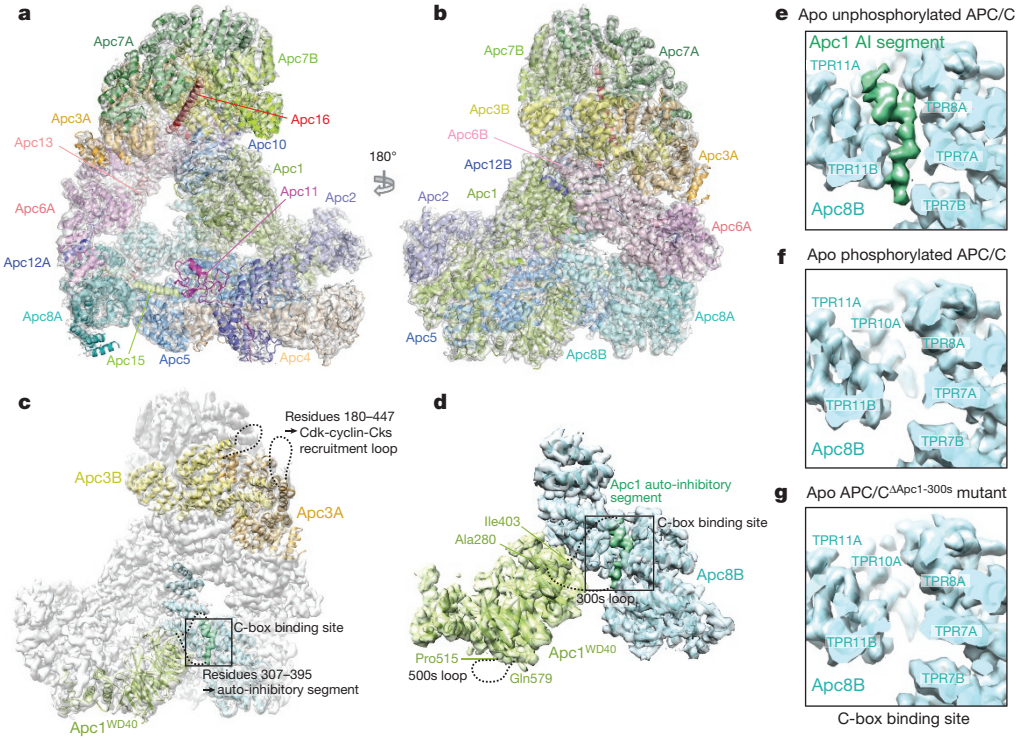

Figure 2 | Apo unphosphorylated APC/C is repressed by an Apc1 auto-inhibitory segment. a, **b**, Two views of the phosphorylated apo APC/C structure in cartoon within the 3.4 Å EM map (grey). The catalytic module (Apc2 and Apc11) is in the inactive conformation. **c**, **d**, EM map of unphosphorylated apo APC/C. Apc1 has two highly phosphorylated loops within its WD40 domain (green). Whereas the 300s loop (residues 307–395) is pointing towards the Apc1 auto-inhibitory segment density (dark green) at the C-box binding site (black box), the 500s loop is facing in the opposite direction. The hyperphosphorylated Apc3 loop (residues 180–447) is located at the back of the APC/C and functions as a Cdk recruitment site. The views in **b** and **c** are similar to Fig. 1b. **e**–**g**, Close-up views of the C-box binding site in the EM maps of apo unphosphorylated and phosphorylated APC/C and an APC/C$^{\Delta Apc1\text{-}300s}$ mutant with the Apc1 300s loop deleted. An elongated loop density (dark green) for the Apc1 auto-inhibitory (AI) segment was observed in the apo unphosphorylated state (**e**), but the density is absent in apo phosphorylated APC/C (**f**). Deletion of the Apc1 300s loop shows a similar loss of C-box site-associated density (**g**).

phosphorylation[18], and interacts with Apc3 (refs 18,27,28), we tested whether Apc3 phosphorylation also had a role in APC/C activation. In Apc3 about 50 phosphorylation sites are clustered in a large disordered loop comprising residues 180–450 (Extended Data Table 2) located on the same face of the APC/C as the Apc1 300s loop (Fig. 2c). In contrast to APC/C$^{\Delta Apc1\text{-}300s}$, instead of stimulating unphosphorylated APC/C, deletion of the Apc3 loop (APC/C$^{\Delta Apc3\text{-}loop}$) reduced the phosphorylation-mediated activation of APC/C (Fig. 3a, lanes 10–13). Similarly, Cdk2–cyclin A3 failed to stimulate the APC/C activity in the absence of Cks2 (Extended Data Fig. 1b). However, combining deletions of both the Apc3 and Apc1 300s loops (APC/C$^{\Delta Apc1\text{-}300s;Apc3\text{-}loop}$) restored activity to that of wild-type phosphorylated APC/C (Fig. 3a, lanes 14, 15). Since deletion of the Apc3 loop disrupts APC/C association with Cdk–cyclin–Cks (Extended Data Fig. 1c, lanes 6, 8), a likely explanation for our results and for the lag phase that accompanies APC/C activation by Cdk1–cyclin B–Cks[19], is that Apc3 phosphorylation recruits Cdk–cyclin–Cks through Cks[18,27,28] to stimulate Apc1 auto-inhibitory segment phosphorylation. Cdk–cyclin–Cks association with the Apc3 loop would allow for a kinetically more efficient intra-molecular phosphorylation of the Apc1 auto-inhibitory segment that only becomes accessible to Cdk when transiently displaced from the C-box site (Figs 3c and 4a).

To determine whether Apc3 loop-mediated interactions with the Cks2 subunit facilitated Apc1 300s loop phosphorylation, we analysed phosphorylation of the Apc1 300s loop in conditions where such interactions are disrupted. Either deletion of the Apc3 loop or omission of the Cks2 subunit from the phosphorylation reaction, conditions that reduce APC/C activation (Fig. 3a and Extended Data Fig. 1b), resulted in the same reduction of Apc1 300s loop phosphorylation (Extended Data Table 2). Specifically, mitotic phospho-sites associated with relief of auto-inhibition (Ser364, Ser372 and Ser373) (Extended Data Table 2, columns 3 and 8) are not modified when Cdk targeting to Apc3 is disrupted (Extended Data Table 2, columns 4 and 5). In agreement with[12,22] Ser362 and Ser364 are phosphorylated by Plk1 and Cdk2–cyclin A3–Cks2, respectively, indicating that Ser364 phosphorylation confers partial activation, whereas phosphorylation of Ser372 and Ser373 requires the presence of both kinases, possibly owing to interdependent priming reactions. Since the stimulatory phospho-Ser364 of the auto-inhibitory segment (Fig. 3c) is a non Cdk-consensus site, the relaxed specificity of Cdk2–cyclin A3–Cks2 phosphorylation of this site may be conferred through targeting of the kinase to the APC/C through the Apc3 loop.

Cdc20 and Cdh1 bind to common sites on the APC/C yet only Cdc20 association is regulated by APC/C phosphorylation. In agreement with ref. 9, we find that Cdh1 activates unphosphorylated and phosphorylated APC/C to a similar extent (Extended Data Fig. 6d, e). Comparing unphosphorylated APC/C and APC/C$^{\Delta Apc1\text{-}300s}$ we detect some stimulation with APC/C$^{\Delta Apc1\text{-}300s}$ at low Cdh1 concentrations (Extended Data Fig. 6e). This is consistent with the enhancement of Cdh1 binding to phosphorylated APC/C and APC/C$^{\Delta Apc1\text{-}300s}$ (Extended Data Fig. 6b). Testing the phosphorylation-dependent activity of a set of Cdc20-Cdh1 chimaeras indicated that the more extensive interactions involving Cdh1 and the APC/C, mediated by both Cdh1^{NTD} and Cdh1^{IR} (Extended Data Fig. 6d), with a contribution from the Cdh1^{NTD} α3 helix (Fig. 1c and Extended Data Fig. 6f), account for the capacity of Cdh1 to activate unphosphorylated APC/C. Although Cdh1 association would also require displacement of the Apc1 auto-inhibitory segment, a potential mechanism to explain the dependency of Cdc20 on APC/C phosphorylation is that the higher affinity of Cdh1 for the

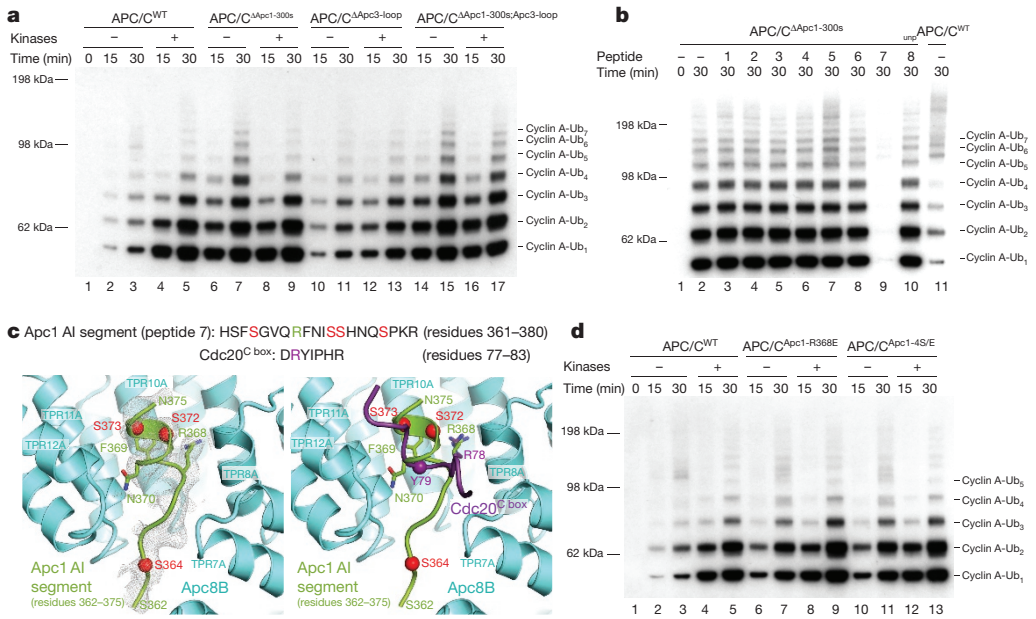

Figure 3 | The Apc1 auto-inhibitory segment binds to the C-box binding site and mimics the Cdc20$^{C\ box}$. **a**, A native substrate Cdk2–cyclin A2–Cks2 was used for ubiquitination assays. *In vitro* phosphorylated APC/C (both Cdk2–cyclin A3–Cks2 and Plk1) can be activated by Cdc20 (lanes 1–5). Deletion of the Apc1 300s loop activated the APC/C without phosphorylation (lanes 6, 7), and kinase treatment of APC/C$^{\Delta Apc1\text{-}300s}$ did not enhance APC/C activity. The APC/C$^{\Delta Apc3\text{-}loop}$ mutant showed similar activity as unphosphorylated APC/C (lanes 10, 11 versus 2, 3 and 4, 5), but had reduced activation by phosphorylation. Nevertheless, deletion of both Apc1 300s and Apc3 loops (APC/C$^{\Delta Apc1\text{-}300s;Apc3\text{-}loop}$) restored activity to that of wild-type (WT) phosphorylated APC/C and unphosphorylated APC/C$^{\Delta Apc1\text{-}300s}$ (lanes 14–17). **b**, Identification of the Apc1 auto-inhibitory segment occupying the C-box binding site by assessing the inhibitory effect of eight peptides spanning the Apc1 300s loop. A single peptide (peptide 7, residues 361–380) suppressed the activity of APC/C$^{\Delta Apc1\text{-}300s}$ (lane 9), indicating that this peptide blocks the C-box binding site. A control with wild-type unphosphorylated APC/C ($_{unp}$APC/C^{WT}) is in lane 11. **c**, The Apc1 auto-inhibitory (AI) segment (peptide 7, residues 361–380) shares sequence similarity with Cdc20$^{C\ box}$. A model for the auto-inhibitory segment (green) was fitted into the EM density of the apo unphosphorylated APC/C map (grey). Arg368 overlaps with the crucial Arg78 of Cdc20$^{C\ box}$ (purple, right panel). The flanking serines shown to be phosphorylated are highlighted as red spheres. Ser377 is outside the observed EM density. **d**, Mutation of a single Arg368 residue (APC/C$^{Apc1\text{-}R368E}$) or mutating its four neighbouring serine residues (Ser364, Ser372, Ser373, Ser377) to glutamates (APC/C$^{Apc1\text{-}4S/E}$) activated the APC/C without phosphorylation. 30 nM Cdc20 was used for the assay in **a** and 20 nM Cdc20 for the assays in **b** and **d**. Experiments in **a** and **d** were replicated three times and in **b** five times. See Supplementary Fig. 1 for gel source data.

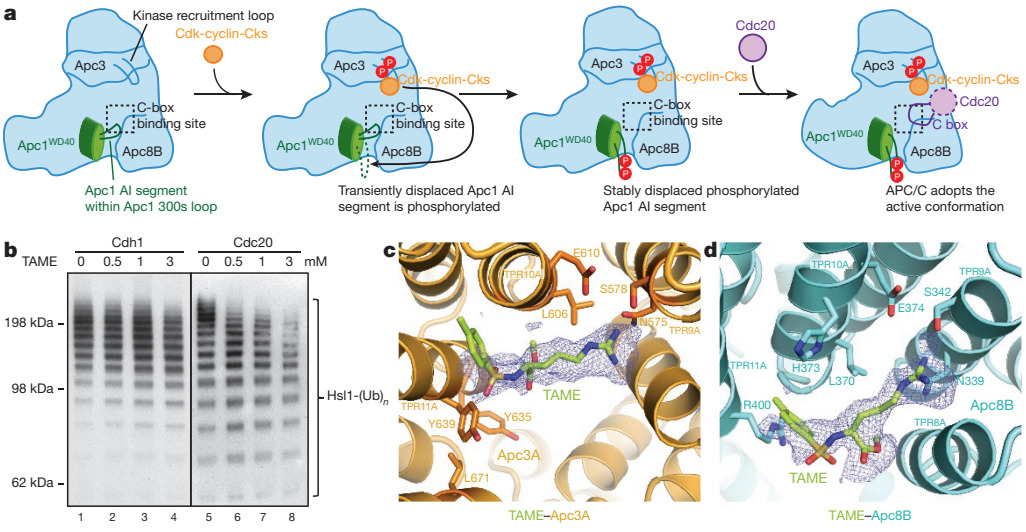

Figure 4 | Mechanism for APC/C activation by mitotic phosphorylation and the molecular basis for TAME inhibition. **a**, Cartoon showing the mechanism of APC/C activation by Apc1 and Apc3 phosphorylation-induced relief of auto-inhibition. Artificial relief of auto-inhibition, either by deletion of the Apc1 auto-inhibitory (AI) segment or by its phospho-mimicking mutants, obviates the need to phosphorylate Apc3. **b**, TAME has only a small inhibitory effect on APC/C^{Cdh1} (lanes 1–4), whereas it markedly reduced APC/C^{Cdc20} activity (lanes 5–8). The activity assay was performed with phosphorylated wild-type (WT) APC/C and substrate Hsl1 at a coactivator concentration of 10 nM. This experiment was replicated three times. See Supplementary Fig. 1 for gel source data. **c**, **d**, EM reconstruction of APC/C$^{\Delta Apc1\text{-}300s}$ in complex with TAME showed densities (dark blue) for TAME (C-atoms in lime green) at both the IR tail-binding site (**c**), and the C-box binding site (**d**). Their positions overlap well with the crucial Arg78 and Tyr79 of Cdc20$^{C\ box}$ and Ile498 and Arg499 of Cdc20^{IR}, thereby inhibiting Cdc20 association (Extended Data Fig. 7).

APC/C (Extended Data Fig. 6e) is sufficient to compete for the auto-inhibitory segment at the C-box binding site.

Our findings suggest the interesting possibility of exploiting differences in the affinities of the two coactivators for the design of inhibitors that specifically target mitotic APC/C^{Cdc20} and thus suppress cell proliferation. A small molecule, tosyl-L-arginine methyl ester (TAME), was reported to inhibit APC/C activation by both Cdc20 and Cdh1 through a proposed mechanism involving competition for the IR tail-binding site of coactivator[29]. However, we found that TAME is a more potent inhibitor of APC/C^{Cdc20} than APC/C^{Cdh1} (Fig. 4b). To understand the molecular basis underlying this inhibition, we determined the structure of APC/C$^{\Delta Apc1\text{-}300s}$ in complex with TAME (Extended Data Table 1). We observed TAME density not only at the IR tail-binding site, but also at the C-box binding site (Fig. 4c, d). This is consistent with the structural similarities of the IR tail and C-box bindings sites of Apc3A and Apc8B, respectively[23], although there are critical differences. In Apc3A, TAME is reminiscent of the Ile–Arg motif of the coactivator IR tail, whereas in Apc8B, TAME resembles the Arg–Tyr/Phe of the coactivator C box (Extended Data Fig. 7). The mechanism of TAME inhibition of APC/C^{Cdc20} through a tosyl-Arg motif to block the Cdc20$^{C\ box}$ binding site is reminiscent of the Apc1 auto-inhibitory segment that is displaced by APC/C phosphorylation. Both utilize a common structural motif (Arg-aromatic) that mimics Arg78 and Tyr79 of Cdc20$^{C\ box}$ to exploit the lower (relative to Cdh1) affinity of Cdc20 for the APC/C.

How phosphorylation regulates mitotic APC/C activation by Cdc20 has been a long-standing puzzle. Our *in vitro* studies show that of almost 150 phosphorylation sites in mitotic APC/C, only a few in Apc1 directly regulate Cdc20 binding through displacement of the auto-inhibitory segment. This work has relevance to understanding the control of other large multimeric complexes by multi-site phosphorylation.

Online Content Methods, along with any additional Extended Data display items and Source Data, are available in the online version of the paper; references unique to these sections appear only in the online paper.

Received 15 December 2015; accepted 6 April 2016.
Published online 27 April 2016.

1. Pines, J. Cubism and the cell cycle: the many faces of the APC/C. *Nat. Rev. Mol. Cell Biol.* **12,** 427–438 (2011).
2. Primorac, I. & Musacchio, A. *Panta rhei*: the APC/C at steady state. *J. Cell Biol.* **201,** 177–189 (2013).
3. Chang, L. & Barford, D. Insights into the anaphase-promoting complex: a molecular machine that regulates mitosis. *Curr. Opin. Struct. Biol.* **29,** 1–9 (2014).
4. Kimata, Y., Baxter, J. E., Fry, A. M. & Yamano, H. A role for the Fizzy/Cdc20 family of proteins in activation of the APC/C distinct from substrate recruitment. *Mol. Cell* **32,** 576–583 (2008).
5. Van Voorhis, V. A. & Morgan, D. O. Activation of the APC/C ubiquitin ligase by enhanced E2 efficiency. *Curr. Biol.* **24,** 1556–1562 (2014).
6. Chang, L., Zhang, Z., Yang, J., McLaughlin, S. H. & Barford, D. Molecular architecture and mechanism of the anaphase-promoting complex. *Nature* **513,** 388–393 (2014).
7. Lahav-Baratz, S., Sudakin, V., Ruderman, J. V. & Hershko, A. Reversible phosphorylation controls the activity of cyclosome-associated cyclin-ubiquitin ligase. *Proc. Natl Acad. Sci. USA* **92,** 9303–9307 (1995).
8. Shteinberg, M., Protopopov, Y., Listovsky, T., Brandeis, M. & Hershko, A. Phosphorylation of the cyclosome is required for its stimulation by Fizzy/cdc20. *Biochem. Biophys. Res. Commun.* **260,** 193–198 (1999).
9. Kramer, E. R., Scheuringer, N., Podtelejnikov, A. V., Mann, M. & Peters, J. M. Mitotic regulation of the APC activator proteins CDC20 and CDH1. *Mol. Biol. Cell* **11,** 1555–1569 (2000).
10. Rudner, A. D. & Murray, A. W. Phosphorylation by Cdc28 activates the Cdc20-dependent activity of the anaphase-promoting complex. *J. Cell Biol.* **149,** 1377–1390 (2000).
11. Golan, A., Yudkovsky, Y. & Hershko, A. The cyclin-ubiquitin ligase activity of cyclosome/APC is jointly activated by protein kinases Cdk1-cyclin B and Plk. *J. Biol. Chem.* **277,** 15552–15557 (2002).
12. Kraft, C. *et al.* Mitotic regulation of the human anaphase-promoting complex by phosphorylation. *EMBO J.* **22,** 6598–6609 (2003).
13. Zachariae, W., Schwab, M., Nasmyth, K. & Seufert, W. Control of cyclin ubiquitination by CDK-regulated binding of Hct1 to the anaphase promoting complex. *Science* **282,** 1721–1724 (1998).
14. Jaspersen, S. L., Charles, J. F. & Morgan, D. O. Inhibitory phosphorylation of the APC regulator Hct1 is controlled by the kinase Cdc28 and the phosphatase Cdc14. *Curr. Biol.* **9,** 227–236 (1999).
15. Schwab, M., Neutzner, M., Möcker, D. & Seufert, W. Yeast Hct1 recognizes the mitotic cyclin Clb2 and other substrates of the ubiquitin ligase APC. *EMBO J.* **20,** 5165–5175 (2001).
16. Passmore, L. A. *et al.* Doc1 mediates the activity of the anaphase-promoting complex by contributing to substrate recognition. *EMBO J.* **22,** 786–796 (2003).
17. Vodermaier, H. C., Gieffers, C., Maurer-Stroh, S., Eisenhaber, F. & Peters, J. M. TPR subunits of the anaphase-promoting complex mediate binding to the activator protein CDH1. *Curr. Biol.* **13,** 1459–1468 (2003).
18. Patra, D. & Dunphy, W. G. Xe-p9, a *Xenopus* Suc1/Cks protein, is essential for the Cdc2-dependent phosphorylation of the anaphase- promoting complex at mitosis. *Genes Dev.* **12,** 2549–2559 (1998).
19. Shteinberg, M. & Hershko, A. Role of Suc1 in the activation of the cyclosome by protein kinase Cdk1/cyclin B. *Biochem. Biophys. Res. Commun.* **257,** 12–18 (1999).
20. Herzog, F., Mechtler, K. & Peters, J. M. Identification of cell cycle-dependent phosphorylation sites on the anaphase-promoting complex/cyclosome by mass spectrometry. *Methods Enzymol.* **398,** 231–245 (2005).
21. Steen, J. A. *et al.* Different phosphorylation states of the anaphase promoting complex in response to antimitotic drugs: a quantitative proteomic analysis. *Proc. Natl Acad. Sci. USA* **105,** 6069–6074 (2008).
22. Hegemann, B. *et al.* Systematic phosphorylation analysis of human mitotic protein complexes. *Sci. Signal.* **4,** rs12 (2011).
23. Chang, L., Zhang, Z., Yang, J., McLaughlin, S. H. & Barford, D. Atomic structure of the APC/C and its mechanism of protein ubiquitination. *Nature* **522,** 450–454 (2015).
24. Herzog, F. *et al.* Structure of the anaphase-promoting complex/cyclosome interacting with a mitotic checkpoint complex. *Science* **323,** 1477–1481 (2009).
25. Izawa, D. & Pines, J. Mad2 and the APC/C compete for the same site on Cdc20 to ensure proper chromosome segregation. *J. Cell Biol.* **199,** 27–37 (2012).
26. Yamaguchi, M. *et al.* Structure of an APC3-APC16 complex: insights into assembly of the anaphase-promoting complex/cyclosome. *J. Mol. Biol.* **427,** 1748–1764 (2015).
27. van Zon, W. *et al.* The APC/C recruits cyclin B1-Cdk1-Cks in prometaphase before D box recognition to control mitotic exit. *J. Cell Biol.* **190,** 587–602 (2010).
28. Sudakin, V., Shteinberg, M., Ganoth, D., Hershko, J. & Hershko, A. Binding of activated cyclosome to p13(suc1). Use for affinity purification. *J. Biol. Chem.* **272,** 18051–18059 (1997).
29. Zeng, X. *et al.* Pharmacologic inhibition of the anaphase-promoting complex induces a spindle checkpoint-dependent mitotic arrest in the absence of spindle damage. *Cancer Cell* **18,** 382–395 (2010).

Supplementary Information is available in the online version of the paper.

Acknowledgements This work was funded by the MRC Laboratory of Molecular Biology and a Cancer Research UK grant to D.B. PhD funding for S.Z. was from the Gates Cambridge Scholarship and Boehringer Ingelheim Fonds. C.A. is an EMBO Fellow. We are grateful to members of the Barford group for discussion; S. Chen, C. Savva and G. McMullan for EM facilities; J. Grimmet and T. Darling for computing; K. Zhang for advice on data processing; G. Murshudov for help with REFMAC and S. Aibara for advice on cloning.

Author Contributions S.Z. cloned the substrates and Cdh1 mutant, purified proteins and performed biochemical analysis. S.Z. and L.C. prepared grids, collected and analysed EM data and determined the three-dimensional reconstructions. S.Z. fitted coordinates, built models and made figures with help of L.C. C.A. cloned kinases and Cdc20 and established *in vitro* phosphorylation of the APC/C. Z.Z. and J.Y. cloned the APC/C mutants and the chimaeric proteins and prepared viruses. S.M. and M.S. performed mass spectrometry. D.B. directed the project and designed experiments with S.Z. S.Z. and D.B. wrote the manuscript with input from authors.

Author Information EM maps are deposited in the Electron Microscopy Data Bank with accession codes 3385 (APC/C$^{Cdc20\text{-}Hsl1}$), 3386 (apo unphosphorylated APC/C), 3387 (apo phosphorylated APC/C), 3388 (combined apo phosphorylated APC/C), 3389 (APC/C$^{\Delta Apc1\text{-}300s}$) and 3390 (APC/C$^{\Delta Apc1\text{-}300s\text{-}TAME}$). Protein coordinates are deposited in the Protein Data Bank under accession codes 5G04 (APC/C$^{Cdc20\text{-}Hsl1}$) and 5G05 (apo phosphorylated APC/C). Reprints and permissions information is available at www.nature.com/reprints. The authors declare no competing financial interests. Readers are welcome to comment on the online version of the paper. Correspondence and requests for materials should be addressed to D.B. (dbarford@mrc-lmb.cam.ac.uk).

METHODS

No statistical methods were used to predetermine sample size. The experiments were not randomized and the investigators were not blinded to allocation during experiments and outcome assessment.

Expression and purification of recombinant human APC/C. The genes for recombinant human APC/C were cloned into a modified MultiBac system, expressed and purified as described[30]. The C terminus of Apc4 was fused to a TEV (tobacco etch virus)-cleavable StrepII×2 tag.

Protein kinase purification. All four proteins (Cdk2, cyclin A3 (residues 174–432), Cks2 and Plk1 (residues 37–338)) for the kinases were expressed individually in BL21 (DE3) Star cells at 18 °C overnight. Pellets containing GST-tagged Cdk2, His-tagged cyclin A3 and His-SUMO-tagged Cks2 were combined and resuspended in the CDK lysis buffer (50 mM Tris/HCl pH 7.4, 180 mM NaCl, 5% glycerol and 2 mM DTT) supplemented with 0.1 mM PMSF, lysozyme, 5 units per ml benzonase and Complete EDTA-free protease inhibitors (Roche). After sonication, the cells were centrifuged at 20,000 r.p.m. for 1 h at 4 °C and the supernatant was incubated with the Glutathione Sepharose 4B (GE Healthcare) for 3 h at 4 °C. The resins were washed with the CDK lysis buffer and the GST-tag of Cdk2 was cleaved off with 3C PreScission protease overnight at 4 °C. The flow-through from the resins was collected and TEV-cleaved overnight at 4 °C. Finally, the protein complex was purified by a Superdex200 16/60 column (GE Healthcare).

The Polo kinase Plk1 with an N-terminal His-MBP tag was purified with a HisTrap HP column (GE Healthcare) in the PLK lysis buffer (50 mM Tris/HCl pH 7.5, 300 mM NaCl, 20 mM imidazole, 5% glycerol and 2 mM β-mercaptoethanol). The column was washed intensively with high-salt buffer (50 mM Tris/HCl pH 7.5, 1 M NaCl, 20 mM imidazole, 5% glycerol and 2 mM β-mercaptoethanol). Proteins were eluted with a gradient of the elution buffer (50 mM Tris/HCl pH 7.5, 300 mM NaCl, 300 mM imidazole, 5% glycerol and 2 mM β-mercaptoethanol) followed by TEV-cleavage overnight at 4 °C. The sample was re-applied onto the HisTrap HP column to remove the His tag, uncleaved proteins and nickel contaminations. The collected flow-through was concentrated and loaded onto a Superdex75 16/60 column (GE Healthcare) for final purification.

***In vitro* phosphorylation of recombinant human APC/C.** Concentrated APC/C after Resource Q (GE Healthcare) was treated with Cdk2–cyclin A3–Cks2 and Plk1 in a molar ratio of 1:1.5 (APC/C: kinases) in a reaction buffer of 40 mM HEPES pH 8.0, 10 mM $MgCl_2$ and 0.6 mM DTT with 5 mM ATP and 50 mM NaF. The reaction mixture was incubated at 30 °C for 30 min before the final purification step by a Superose 6 3.2/300 column (GE Healthcare) in the APC/C gel-filtration buffer (20 mM HEPES pH 8.0, 150 mM NaCl, 0.5 mM TCEP).

Expression and purification of the substrate Cdk2–cyclin A2–Cks2 and Cdc20. Full-length human cyclin A2 was cloned into the pETM41 vector with an N-terminal His-MBP tag. The protein was expressed in BL21 (DE3) Star cells at 18 °C overnight. Pellets containing Cdk2, cyclin A2 and Cks2 were co-lysed for purification following a similar protocol as for the kinase purification.

Full-length human Cdc20 was cloned into a modified pFastBac HTa vector with an N-terminal His-MBP tag. The generated virus was amplified and expressed in Sf9 cells. Harvested cell pellets were resuspended in Cdc20 lysis buffer (50 mM HEPES pH 7.8, 500 mM NaCl, 30 mM imidazole, 10% glycerol and 0.5 mM TCEP) supplemented with 0.1 mM PMSF, 5 units per ml benzonase and Complete EDTA-free protease inhibitors and loaded onto a HisTrap HP column (GE Healthcare). Proteins were eluted with a gradient to 300 mM imidazole. Collected peak fractions were TEV-cleaved overnight in the dialysis bag (cut-off 6–8 kDa) against the dialysis buffer (50 mM HEPES, pH 7.8, 300 mM NaCl, 5% glycerol and 0.5 mM TCEP) at 4 °C. The protein was re-applied onto the HisTrap HP column and the flow-through was collected.

Complex formation of APC/$C^{Cdc20\text{-}Hsl1}$ and APC/$C^{\Delta Apc1\text{-}300s\text{-}TAME}$. *In vitro* phosphorylated APC/C was treated with 40 μM CDK1/2 inhibitor III (ENZO Life Sciences) before incubating with purified Cdc20 and Hsl1 (with a molar ratio of 1:1.5:2) on ice. The complex was purified by a Superose 6 3.2/300 column using the Microakta system.

TAME (Sigma-Aldrich) was dissolved in 50% DMSO and 50% APC/C gel-filtration buffer at a concentration of 1 M. 4 mM TAME was added to purified APC/$C^{\Delta Apc1\text{-}300s}$ and incubated on ice for 1 h before freezing cryo-grids.

Ubiquitination assays. The ubiquitination assay was performed with 60 nM recombinant human APC/C, 90 nM UBA1, 300 nM UbcH10, 300 nM Ube2S, 70 μM ubiquitin, 2 μM substrate Cdk2–cyclin A2–Cks2 or Hsl1, 5 mM ATP, 0.25 mg ml^{-1} BSA, 15 μM CDK1/2 inhibitor III and different concentrations of purified human Cdc20 (5–30 nM) or Cdh1 (5–30 nM) in a 10 μl reaction volume with 40 mM HEPES pH 8.0, 10 mM $MgCl_2$ and 0.6 mM DTT (figure legends indicate the exact coactivator concentration used in each assay). Reaction mixtures were incubated at room temperature for various time points and terminated by adding SDS/PAGE loading dye. Reactions were analysed by 4–12% NuPAGE Bis-Tris gels followed by western blotting with an antibody against the His-tag of ubiquitin (Clonetech cat. code: 631212).

For the chimaeric Cdh1-Cdc20 assay, the following domain boundaries were used to generate chimaeric Cdh1-Cdc20 proteins: $Cdh1^{NTD}$ (residues 1–168), $Cdh1^{WD40}$ (residues 169–475), $Cdh1^{IR}$ (residues 476–496), $Cdc20^{NTD}$ (residues 1–165), $Cdc20^{WD40}$ (residues 166–475), $Cdc20^{IR}$ (residues 476–499). 10 nM of the chimaeric proteins were used in the assay.

Peptide and TAME assays. Eight peptides (Designer BioScience) spanning the Apc1 300s loop were synthesized for identification of the Apc1 auto-inhibitory segment. Each peptide contains 20 amino acids, with a ten-residue overlap with the neighbouring peptides: peptide 1 (LTAHLRSLSKGDSPVTSPFQ); peptide 2 (GDSPVTSPFQNYSSIHSQSR); peptide 3 (NYSSIHSQSRSTSSPSLHSR); peptide 4 (STSSPSLHSRSPSISNMAAL); peptide 5 (SPSISNMAALSRAHSPALGV); peptide 6 (SRAHSPALGVHSFSGVQRFN); peptide 7 (HSFSGVQRFNISSHNQSPKR) and peptide 8 (ISSHNQSPKRHSISHSPNSN). The following mutant peptides of peptide 7 were used to assess the relief of auto-inhibition: peptide R368E (HSFSGVQEFNISSHNQSPKR), peptide 4S/E (HSFEGVQRFNIEEHNQEPKR) and peptide pS377 (HSFSGVQRFNISSHNQphosphoSPKR). The peptides were dissolved at a concentration of 10 mM in 100% dimethylsulfoxide (DMSO) and diluted using the APC/C gel-filtration buffer. The ubiquitination assay was performed using a final concentration of 200 μM peptide. The TAME assay was performed at a similar condition using 0.5–3 mM TAME and the substrate Hsl1.

Size-exclusion chromatography to assess coactivator binding. Purified APC/C samples (1 mg ml^{-1}) were incubated with either Cdh1 or Cdc20 at a molar ratio of 1:1.5 on ice for 30 min. The sample was spun down at 13,000 r.p.m. for 5 min to remove any precipitates or aggregates before injecting onto a Superose 6 3.2/300 column using the Microakta system. The eluted peak fractions were analysed by SDS–PAGE and western blotting.

Mass spectrometry. Purified proteins were prepared for mass spectrometric analysis by in solution enzymatic digestion, without prior reduction and alkylation. Protein samples were digested with trypsin or elastase (Promega), both at an enzyme to protein ratio of 1:20. The resulting peptides were analysed by nano-scale capillary LC-MS/MS using an Ultimate U3000 HPLC (ThermoScientific Dionex) to deliver a flow of approximately 300 nl min^{-1}. A C18 Acclaim PepMap100 5 μm, 100 μm × 20 mM nanoViper (ThermoScientific Dionex), trapped the peptides before separation on a C18 Acclaim PepMap100 3 μm, 75 μm × 250 mM nanoViper (ThermoScientific Dionex, San Jose, USA). Peptides were eluted with a 90 min gradient of acetonitrile (2% to 50%). The analytical column outlet was directly interfaced via a nano-flow electrospray ionization source, with a hybrid quadrupole orbitrap mass spectrometer (Q-Exactive Plus Orbitrap, ThermoScientific). LC-MS/MS data were then searched against an in-house LMB database using the Mascot search engine (Matrix Science)[31], and the peptide identifications validated using the Scaffold program (Proteome Software Inc.)[32]. All data were additionally interrogated manually.

Electron microscopy. Freshly purified APC/C samples were first visualized by negative-staining EM to check the sample quality and homogeneity and to get initial low-resolution reconstructions. Micrographs were recorded on an FEI Spirit electron microscope at an accelerating voltage of 120 kV and at a defocus of approximately −1.5 μm. For cryo-EM, 2-μl aliquots of the sample at ∼0.15 mg ml^{-1} were applied onto the Quantifoil R2/2 grids coated with a layer of continuous carbon film (approximately 50 Å thick). Grids were treated with a 9:1 argon:oxygen plasma cleaner for 20 to 40 s before use. The grids were incubated for 30 s at 4 °C and 100% humidity before blotting for 5 s and plunging into liquid ethane using an FEI Vitrobot III. The grids were loaded into an FEI Tecnai Polara electron microscope at an acceleration voltage of 300 kV. Micrographs were taken using EPU software (FEI) at a nominal magnification of 78,000 which yields a pixel size of 1.36 Å per pixel. They were recorded by an FEI Falcon III direct electron detector with a defocus range of −2.0 to −4.0 μm. The exposure time for each micrograph was 2 s at a dose rate of 27 electrons per $Å^2$ per s. 34 movie frames were recorded for each micrograph as described[33].

Image processing. All movie frames were aligned by the motioncorr program[34] before subsequent processing. First, the contrast transfer function parameters were calculated with CTFFIND3 or Gctf[35,36]. Particles in 264 pixels × 264 pixels were selected by automatic particle picking in RELION 1.4 (ref. 37). The following steps were performed to exclude bad particles from the data set: (1) automatically picked particles in each micrograph were screened manually to remove ice contaminations[38]; (2) after particle sorting in RELION, particles with poor similarity to reference images were deleted; (3) 2-dimensional classification was performed and particles in bad classes with poorly recognizable features were excluded. The remaining particles were divided into six classes using three-dimensional

classification in RELION. During this process particles with conformational heterogeneity and leftover bad particles were removed from the final reconstruction. After 3D refinement, beam-induced particle motion was corrected using particle polishing in RELION[33,39]. All resolution estimations were based on the gold-standard Fourier shell correlation (FSC) calculations using the FSC = 0.143 criterion. The model for the apo state (Fig. 2a, b, combined apo APC/C structure) was built based on a 3.4 Å resolution map, reconstructed by combined data collected from pure apo phosphorylated APC/C and the apo state particles classified from the APC/C$^{Cdc20\text{-}Hsl1}$ complex (Extended Data Fig. 2 and Extended Data Table 1). This map allowed for model building of regions which were less well-resolved and presented as poly-alanines in the previous APC/C$^{Cdh1\text{-}Emi1}$ structure[23], including Apc2^{NTD}, Apc1 loops in both the WD40 domain and the middle domain and regions in Apc5^{NTD}. A summary of all EM reconstructions obtained in this work is listed in Extended Data Table 1a.

Model building. Model building of both apo APC/C and APC/C$^{Cdc20\text{-}Hsl1}$ structures were performed in COOT[40]. Initially, available atomic structure of human APC/C$^{Cdh1\text{-}Emi1}$ (PDB 4UI9)[23] and the crystal structure of Cdc20^{WD40} (PDB 4GGC)[41] were rigid-body fitted in individual subunits into the cryo-EM maps in Chimera[42]. All fitted structures were rebuilt according to the cryo-EM map. Cdc20^{NTD}, Cdc20^{CTD} and several loop regions not seen in previous structures were built *ab initio*. The models were refined by REFMAC 5.8 (ref. 43). A REFMAC weight of 0.04 was defined by cross-validation using half reconstructions[44]. A resolution limit of 4.0 Å or 3.5 Å was used for the APC/C$^{Cdc20\text{-}Hsl1}$ and the apo APC/C structure, respectively. All available crystal structures or NMR structures were used for secondary structure restraints. The refinement statistics are summarized in Extended Data Table 1b.

Map visualization. Figures were generated using Pymol and Chimera[42].

Sequence alignment. Sequence alignment was performed using Jalview[45].

30. Zhang, Z. *et al.* Recombinant expression, reconstitution and structure of human anaphase-promoting complex (APC/C). *Biochem. J.* **449,** 365–371 (2013).
31. Perkins, D. N., Pappin, D. J., Creasy, D. M. & Cottrell, J. S. Probability-based protein identification by searching sequence databases using mass spectrometry data. *Electrophoresis* **20,** 3551–3567 (1999).
32. Keller, A., Nesvizhskii, A. I., Kolker, E. & Aebersold, R. Empirical statistical model to estimate the accuracy of peptide identifications made by MS/MS and database search. *Anal. Chem.* **74,** 5383–5392 (2002).
33. Bai, X. C., Fernandez, I. S., McMullan, G. & Scheres, S. H. Ribosome structures to near-atomic resolution from thirty thousand cryo-EM particles. *eLife* **2,** e00461 (2013).
34. Li, X. *et al.* Electron counting and beam-induced motion correction enable near-atomic-resolution single-particle cryo-EM. *Nat. Methods* **10,** 584–590 (2013).
35. Mindell, J. A. & Grigorieff, N. Accurate determination of local defocus and specimen tilt in electron microscopy. *J. Struct. Biol.* **142,** 334–347 (2003).
36. Zhang, K. Gctf: real-time CTF determination and correction. *J. Struct. Biol.* **193,** 1–12 (2016).
37. Scheres, S. H. RELION: implementation of a Bayesian approach to cryo-EM structure determination. *J. Struct. Biol.* **180,** 519–530 (2012).
38. Scheres, S. H. Semi-automated selection of cryo-EM particles in RELION-1.3. *J. Struct. Biol.* **189,** 114–122 (2015).
39. Scheres, S. H. Beam-induced motion correction for sub-megadalton cryo-EM particles. *eLife* **3,** e03665 (2014).
40. Emsley, P. & Cowtan, K. Coot: model-building tools for molecular graphics. *Acta Crystallogr. D* **60,** 2126–2132 (2004).
41. Tian, W. *et al.* Structural analysis of human Cdc20 supports multisite degron recognition by APC/C. *Proc. Natl Acad. Sci. USA* **109,** 18419–18424 (2012).
42. Yang, Z. *et al.* UCSF Chimera, MODELLER, and IMP: an integrated modeling system. *J. Struct. Biol.* **179,** 269–278 (2012).
43. Murshudov, G. N. *et al.* REFMAC5 for the refinement of macromolecular crystal structures. *Acta Crystallogr. D* **67,** 355–367 (2011).
44. Fernández, I. S., Bai, X. C., Murshudov, G., Scheres, S. H. & Ramakrishnan, V. Initiation of translation by cricket paralysis virus IRES requires its translocation in the ribosome. *Cell* **157,** 823–831 (2014).
45. Waterhouse, A. M., Procter, J. B., Martin, D. M., Clamp, M. & Barton, G. J. Jalview Version 2–a multiple sequence alignment editor and analysis workbench. *Bioinformatics* **25,** 1189–1191 (2009).

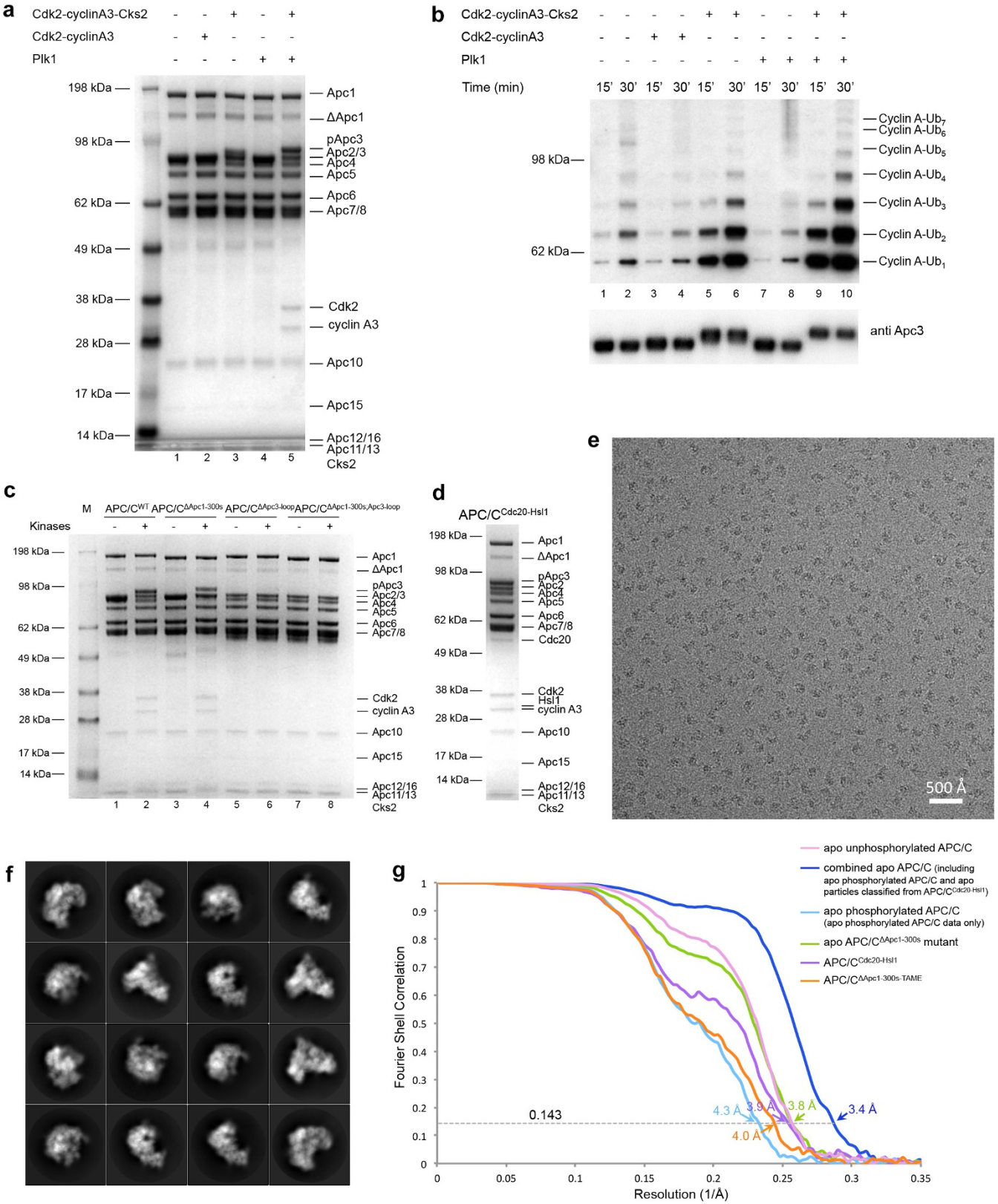

Extended Data Figure 1 | See next page for caption.

Extended Data Figure 1 | Preparations and EM images of different APC/C samples used for structural studies. a, Recombinant human APC/C was phosphorylated *in vitro* using Cdk2–cyclin A3, Cdk2–cyclin A3–Cks2 or Plk1 alone or with both Cdk2–cyclin A3–Cks2 and Plk1. The phosphorylated APC/C samples are shown after SDS–PAGE. **b**, *In vitro* phosphorylated recombinant human APC/C can be fully activated by Cdc20 to ubiquitylate a native substrate Cdk2–cyclin A2–Cks2 when both kinases were added (lanes 9, 10). Without Cks2 (lanes 3, 4) or with Plk1 alone (lanes 7, 8) no activation of the APC/C could be observed, whereas treating with Cdk2–cyclin A3–Cks2 alone (lanes 5, 6) resulted in its partial activation. Samples were recorded at 15 and 30 min of the reaction and 20 nM of Cdc20 was used. This experiment was replicated three times. Anti-Apc3 antibodies (BD Bioscience, cat. code: 610454) were used as a loading control. **c**, Purified wild-type (WT) APC/C and mutant samples with and without kinase treatment (both Cdk2–cyclin A3–Cks2 and Plk1). Upon deletion of the Apc3 loop, no association of the Cdk2–cyclin A3–Cks2 kinase to the APC/C could be observed (lanes 6 and 8). **d**, SDS–PAGE of purified APC/$C^{Cdc20\text{-}Hsl1}$ ternary complex. **e**, A typical cryo-EM micrograph of APC/$C^{Cdc20\text{-}Hsl1}$ representative of 15,582 micrographs. **f**, Gallery of two-dimensional averages of APC/$C^{Cdc20\text{-}Hsl1}$ showing different views; representative of 100 two-dimensional averages. **g**, Gold-standard FSC curves of all APC/C reconstructions in this work. See Supplementary Fig. 1 for gel source data.

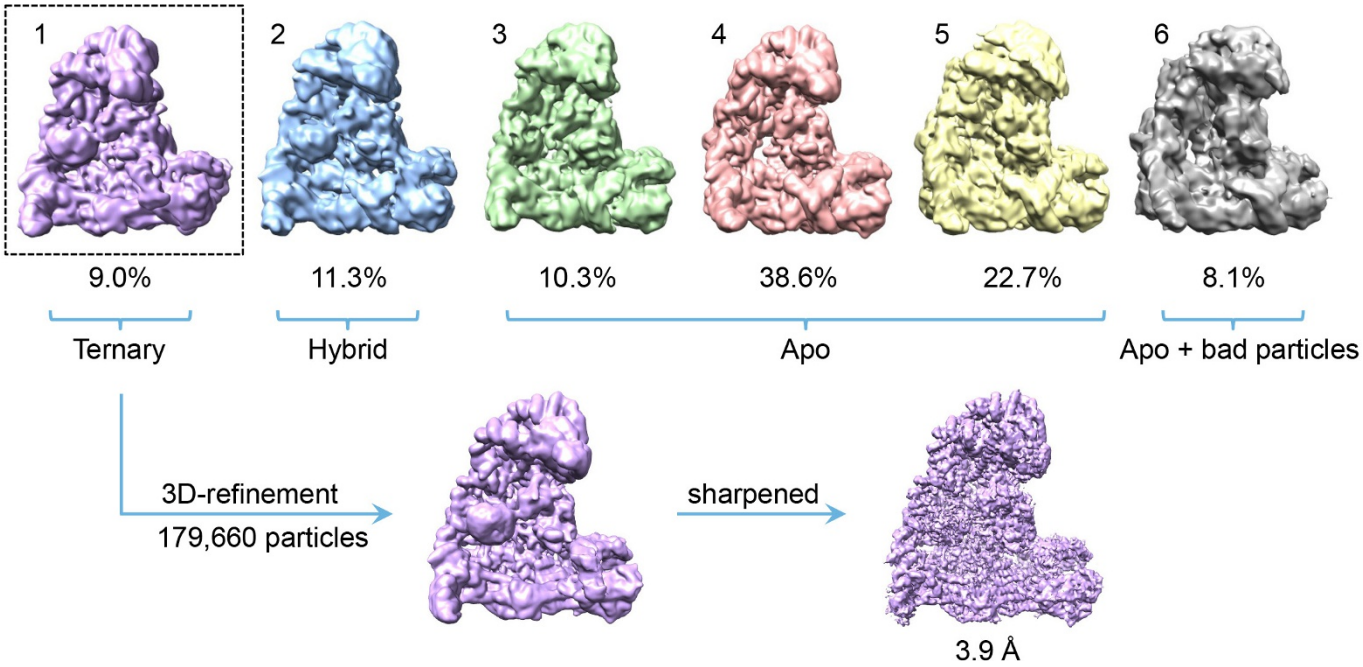

Extended Data Figure 2 | Three-dimensional classification of APC/C$^{Cdc20\text{-}Hsl}$. The initial particles after two-dimensional classification were divided into six classes by three-dimensional classification using RELION. The resultant classes were grouped into four categories: (i) 9.0% in the active ternary state with coactivator and substrate bound; (ii) 11.3% in a hybrid state with coactivator bound, but the APC/C in the inactive conformation; (iii) 71.6% in the inactive apo state; (iv) 8.1% with poorer reconstruction owing to some bad particles. The first class in the active ternary state containing 179,660 particles was used for three-dimensional refinement and movie correction to obtain the final reconstruction at 3.9 Å.

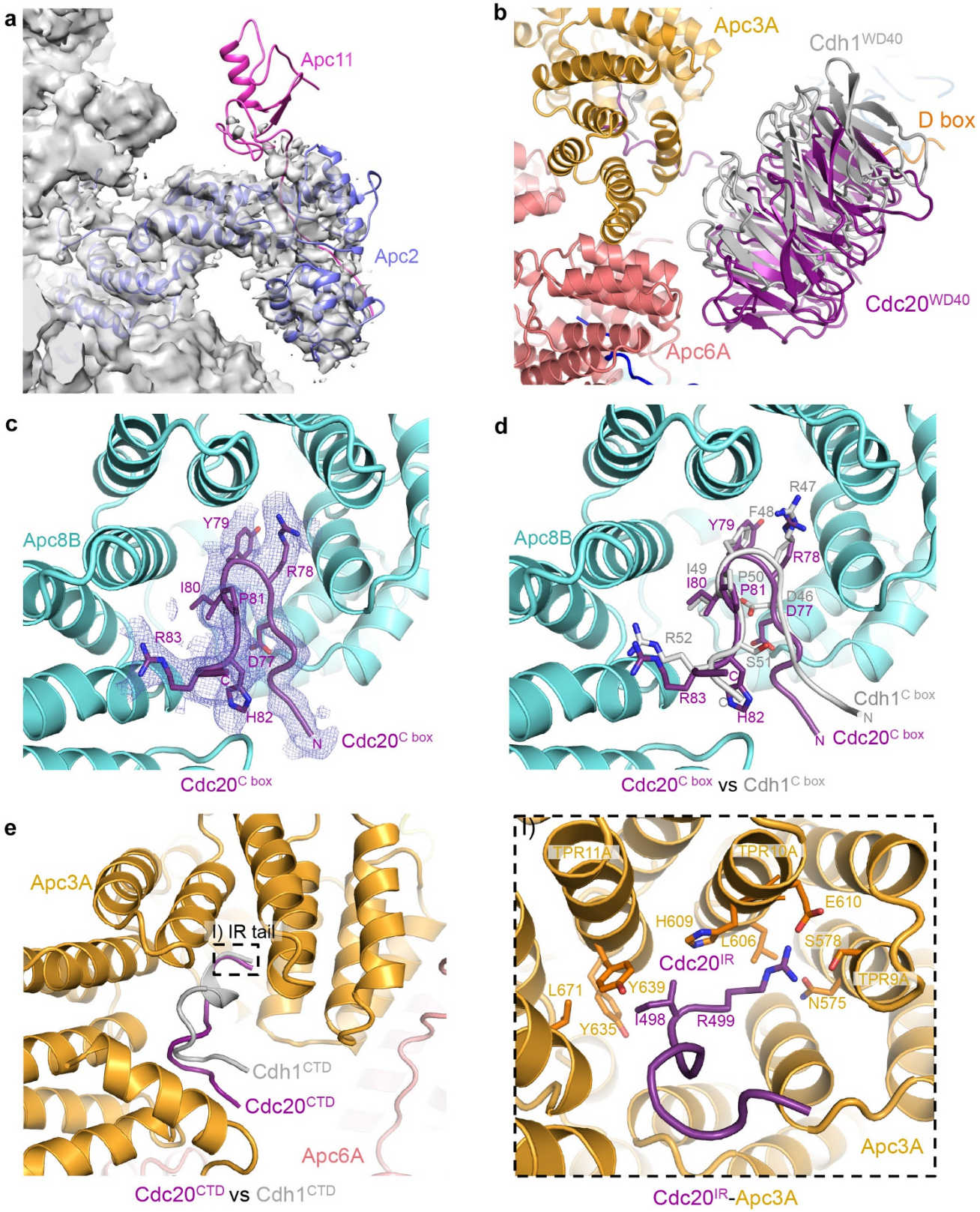

Extended Data Figure 3 | Comparison of Cdc20 and Cdh1 association to the APC/C. a, The catalytic module (Apc2-Apc11) of the APC/$C^{Cdc20\text{-}Hsl1}$ complex is flexible and almost no density accounting for Apc11 (pink, modelled based on the structure of APC/$C^{Cdh1\text{-}Emi1}$, PDB 4UI9)[23] could be observed. **b**, The WD40 domain of Cdc20 (purple) occupies a similar position as $Cdh1^{WD40}$ (grey), but it is displaced from the APC/C by as much as 10 Å. **c**, **d**, EM density for $Cdc20^{C\ box}$ allowed for *ab initio* model building and the C-box interaction with Apc8B (cyan) is well conserved between the two coactivators. **e**, Both $Cdc20^{IR}$ (right) and $Cdh1^{IR}$ (left) associates with Apc3A (orange), although the EM density for $Cdc20^{IR}$ is much weaker (not shown) and the C-terminal α-helix in $Cdh1^{IR}$ is absent.

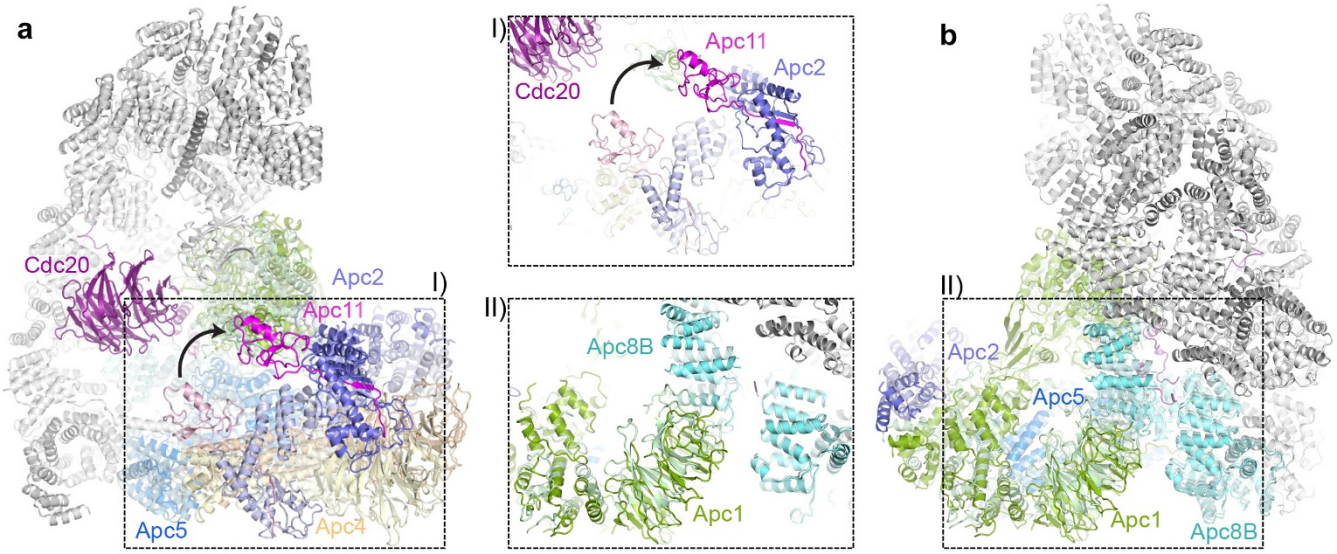

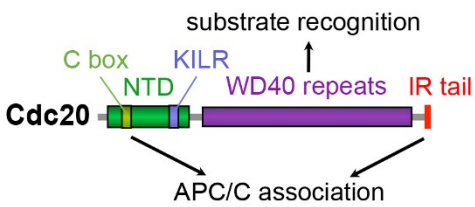

Extended Data Figure 4 | Conformational changes of the APC/C between the inactive apo and the active ternary states and domain and sequence analysis of Cdc20. a, **b**, Subunits that undergo conformational changes upon coactivator and substrate binding are highlighted in their ternary state and coloured as in Fig. 1, while the corresponding proteins in the inactive apo state are in lighter shades. In the active conformation, the platform subdomain containing subunits Apc1, Apc4 and Apc5 is shifted upward, inducing a large movement of the catalytic module to enable E2 access. **c**, Domain organization of Cdc20. **d**, Sequence alignment of $Cdc20^{NTD}$ and $Cdh1^{NTD}$ with α-helices represented as cylinders (purple and grey for $Cdc20^{NTD}$ and $Cdh1^{NTD}$, respectively) underneath the sequences and the C-box and KILR/KLLR motif highlighted.

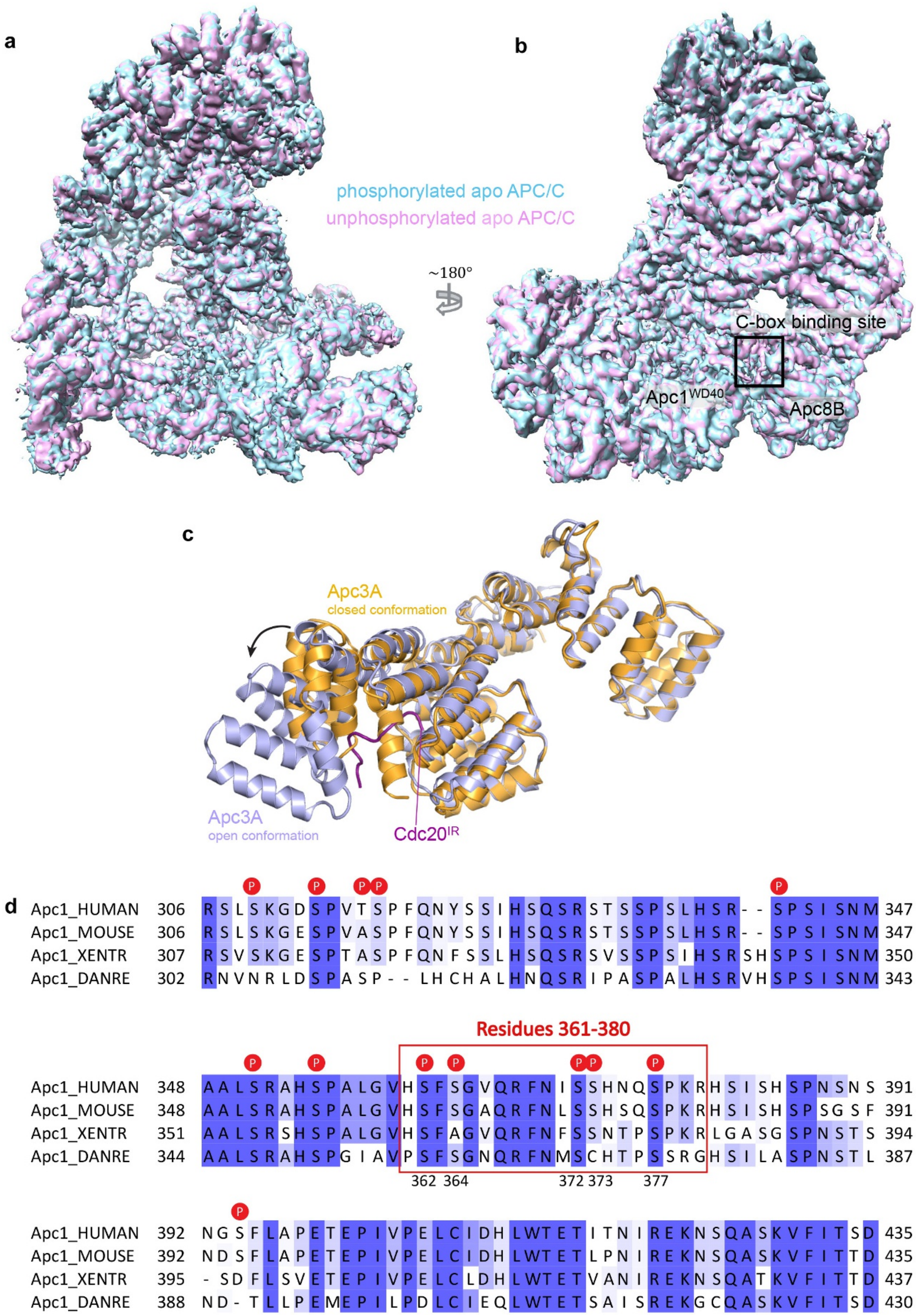

Extended Data Figure 5 | Comparison of apo APC/C in unphosphorylated and phosphorylated states. a, **b**, Superposition of the apo unphosphorylated (magenta) and phosphorylated (cyan) APC/C EM maps revealed little conformational differences except in the vicinity of the C-box binding site. **c**, Apc3A is in an equilibrium between open (light blue) and closed (orange) conformations. While in the inactive apo state, the majority of Apc3A is in the closed state, association of Cdc20^{IR} stabilizes the open state. **d**, Sequence alignment of the Apc1 300s loop across different species human, mouse, *Xenopus tropicalis* (western clawed frog) and *Danio rerio* (zebrafish). Phosphorylation sites are indicated and residues accounting for the Apc1 auto-inhibitory segment (361–380) are boxed.

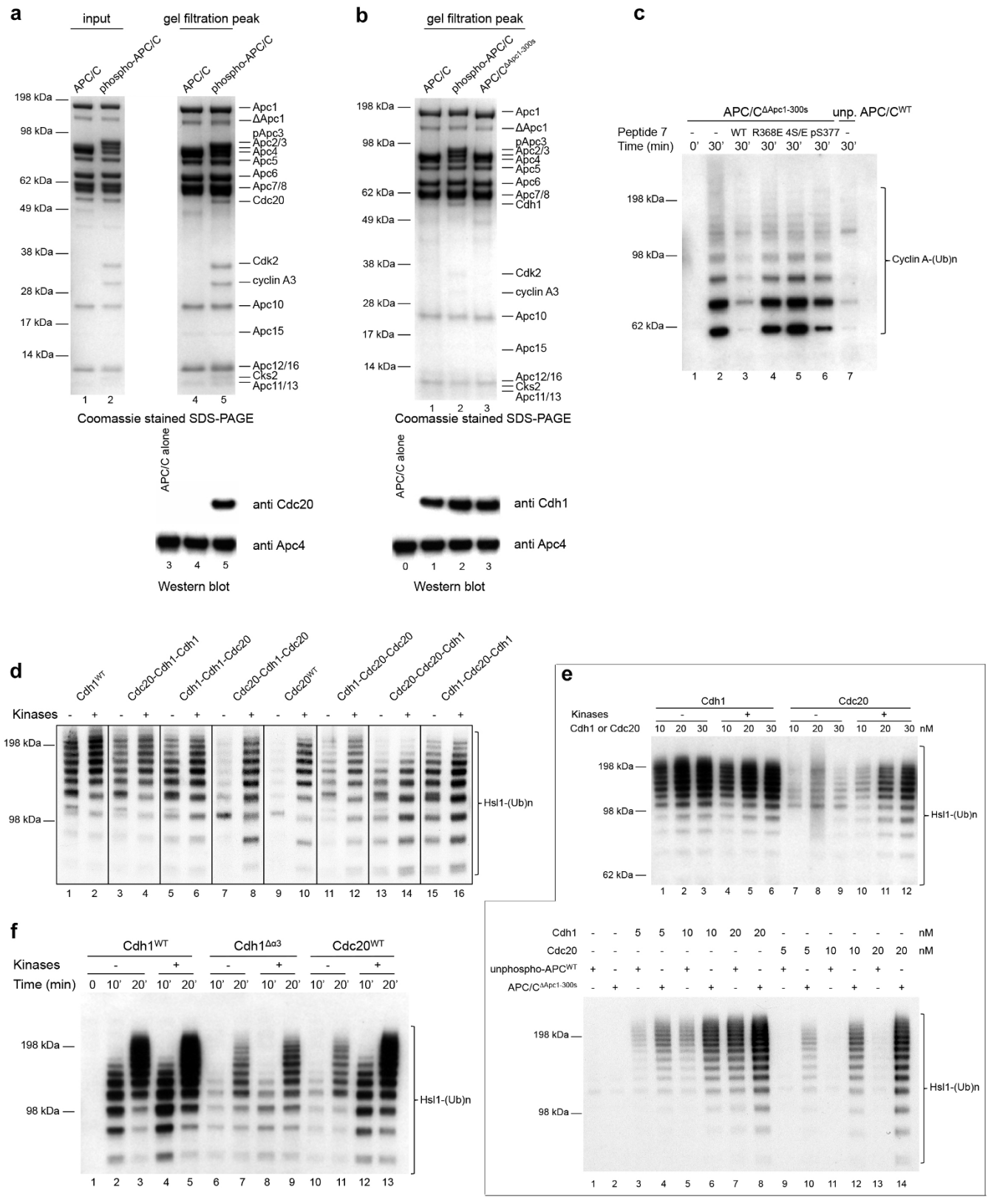

Extended Data Figure 6 | See next page for caption.

Extended Data Figure 6 | Analytical gel filtration and activity assays. **a**, With equal amount of input Cdc20, phosphorylated APC/C could form a stable binary complex with Cdc20 after a gel-filtration purification step (lane 5), whereas unphosphorylated APC/C could not (lane 4). **b**, Both unphosphorylated and phosphorylated APC/C associate with Cdh1 stably on gel filtration, as well as APC/C$^{\Delta Apc1\text{-}300s}$. Anti Cdc20 antibody (Santa Cruz Biotechnology, cat. code: sc-8358) and anti Cdh1 antibody (Sigma, cat. code: C7855) were used for detection; antibody to Apc4 (ref. 6) served as a loading control and unphosphorylated APC/C alone is used as a negative control for western blotting. **c**, Point mutations of peptide 7 (residues 361–380), either when Arg368 was mutated to glutamate or when the four neighbouring serines were mutated to phospho-mimics (Glu), caused the peptide to abolish its inhibition effect and restored the APC/C activity (lanes 4, 5). Phosphorylation of a single Ser377 only resulted in partial activation of the APC/C (lane 6). **d**, Chimaeric proteins composed of the NTD, the WD40 domain and the IR tail of either Cdc20 or Cdh1 were purified to study their differences in APC/C activation. Both the NTD and the CTD of the coactivators are essential for their association with the APC/C. Swapping both NTD and CTD of Cdh1 with Cdc20 makes it phosphorylation sensitive (lanes 7, 8), similar to Cdc20 (lanes 9, 10) and vice versa. **e**, Top, Cdh1 can activate both unphosphorylated and phosphorylated APC/C similarly, whereas Cdc20 requires APC/C phosphorylation for its activity. Bottom, a titration of Cdh1 against unphosphorylated APC/C and APC/C$^{\Delta Apc1\text{-}300s}$ showed enhanced activity in the absence of the Apc1 auto-inhibitory segment at low Cdh1 concentration ($\leq$10 nM), whereas Cdc20 requires displacement of the auto-inhibitory segment for its activity. **f**, Deletion of the Cdh1 α 3 helix resulted in reduced activation of the APC/C and makes Cdh1 more phosphorylation sensitive. The substrate Cdk2–cyclin A2–Cks2 was used for assay in **c** and Hsl1 for the assays in **d–f**. 20 nM Cdc20 was used in **c**, 10 nM chimaeric coactivators in **d** and 30 nM coactivators in **f**. Experiments in **a** and **b** were replicated two times, in **c**, **e** and **f** three times and in **d** four times. See Supplementary Fig. 1 for gel source data.

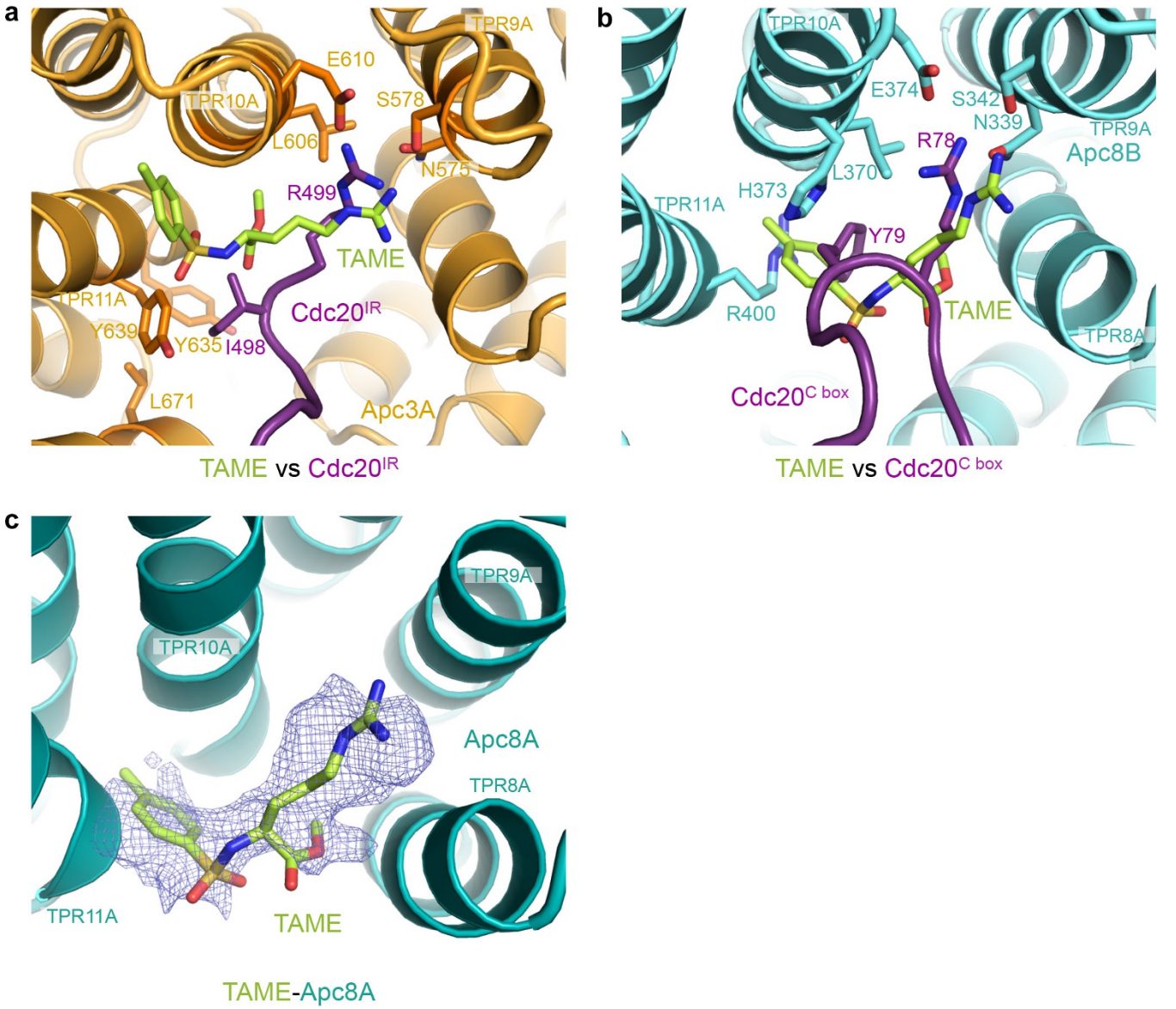

Extended Data Figure 7 | TAME competes with Cdc20 to bind at the IR-tail and the C-box binding sites. a, TAME (C atoms in lime green) is superimposed with Cdc20^{IR} (purple) and the arginine motif in both structures engages the same binding site on Apc3A (orange). **b**, The tosyl-Arg motif of TAME overlaps with Arg78–Tyr79 of Cdc20$^{C\ box}$ at the C-box binding site to out-compete Cdc20. **c**, A density for TAME was also observed within a pocket of the Apc8A TPR super-helix, similar to that of Apc8B.

Extended Data Table 1 | EM data collection, processing statistics and structure refinement statistics

a. Statistics of all cryo-EM reconstructions

Samples	Particles used for final reconstruction	Resolution (Å)	EM-DB accession code
APC/C$^{Cdc20\text{-}Hsl1}$	179,660 (9.0%)	3.9	3385
apo unphosphorylated APC/C	347,317 (49.5%)	3.8	3386
apo phosphorylated APC/C (apo phosphorylated APC/C data only)	83,642 (63.1%)	4.3	3387
combined apo phosphorylated APC/C (both apo phosphorylated APC/C data and apo phosphorylated particles classified from APC/C$^{Cdc20\text{-}Hsl1}$)	921,993 (70.8%)	3.4	3388
apo APC/C$^{\Delta Apc1\text{-}300s}$ mutant	262,090 (80.2%)	3.8	3389
APC/C$^{\Delta Apc1\text{-}300s\text{-}TAME}$	246,065 (78.2%)	4.0	3390

b. Statistics of APC/C$^{Cdc20\text{-}Hsl1}$ and combined apo phosphorylated APC/C structure determination

Data collection	APC/C$^{Cdc20\text{-}Hsl1}$	combined apo phospho. APC/C
EM	FEI Polara, 300k eV	FEI Polara, 300k eV
Detector	FEI Falcon III	FEI Falcon III
Pixel size (Å)	1.36	1.36
Defocus range (μm)	2.0-4.0	2.0-4.0
Reconstruction		
Software	RELION 1.4	RELION 1.4
Accuracy of rotations (degrees)	1.268	0.884
Accuracy of translations (pixels)	0.81	0.62
Final resolution (Å)	3.9	3.4
Refinement		
Software	RefMac 5.8	RefMac 5.8
Refmac weight	0.04	0.04
Resolution limit (Å)	4.0	3.5
Residue number	8164	7908
Average Fourier shell correlation	0.7568	0.7778
R factor	0.3621	0.3451
Rms bond length (Å)	0.0121	0.0141
Rms bond angle (°)	1.7812	1.7435
Validation		
Ramachandran plot		
Preferred	7502 (91.89%)	7427 (93.92%)
Allowed	400 (4.90%)	287 (3.63%)
Outliers	262 (3.21%)	194 (2.45%)
RCSB PDB accession code	5G04	5G05

Extended Data Table 2 | Phosphorylation sites of Apc1 and Apc3 subunits of *in vitro* phosphorylated APC/C identified by mass spectrometry

Protein	Phospho-sites Kinases used	APC/C^{WT} No treatment	APC/C^{WT} Cdk2-cyclinA3	$APC/C^{\Delta Apc3\text{-}loop}$ Cdk2-cyclinA3-Cks2 + Plk1	APC/C^{WT} Cdk2-cyclinA3-Cks2	APC/C^{WT} Plk1	APC/C^{WT} Cdk2-cyclinA3-Cks2 + Plk1	Comparison with published studies Ref.
Apc1	LVGS60LQE							22
	QEVT65IHE							22(interphase)
	PPGS202PRE							12,21,22
	LFGS233SRV	N.D.					N.D.	21
	LKFS286EQG							12,22
	QGGT291PQN							12,21,22
	NVAT297SSS							
	VATS298SSL							
	ATSS299SLT							
	RSLS309KGD			N.D.				22(interphase)
	KGDS313PVT							22
	SPVT316SPF							22
	PVTS317PFQ							22
	HSRS341PSI							12,21,22
	RSPS343ISN							12,22
	AALS351RAH							22
	RAHS355PAL							12,21,22
	GVHS362FSG							12,21,22
	HSFS364GVQ							12,22
	FNIS372SHN							22
	NISS373HNQ							12,22
	HNQS377PKR							12,21,22
	ISHS386PNS						N.D.	22(interphase)
	SPNS389NSN						N.D.	22
	SNGS394FLA							
	WTET416ITN							
	VLYT501GVV							
	PAPS518LTM	N.D.	N.D.	N.D.				22
	PSLT520MSN	N.D.	N.D.					12(interphase),22
	LTMS522NTM	N.D.	N.D.					22(interphase)
	MSNT524MPR	N.D.	N.D.					22(interphase)
	RPST530RLD							12(interphase),21,22
	DGVS536TPK							
	GVST537PKP							12,22
	KPLS542KLL		N.D.					21
	LLGS547LDE							12,22
	VLLS555PVP							12,21,22
	LRDS563SKL							22
	RDSS564KLH	N.D.						21,22
	LHDS569LYN							12(interphase),22
	EDCT576FQQ							
	QLGT582YIH							
	LELS600NGS			N.D.				21
	FEGS686LSP							22
	GSLS688PVI							12,21,22
	ARPS699ETG							22
	PSET701GSD							22
	ETGS703DDD							22(interphase)
	LCLS731PSE							12,22(interphase),21
	NRFS916FRH							22
	FRHS920TSV							
	RHST921SVS							
	HSTS922VSS							
	VLSS1001DVP							
	KHKS1347PSY							
	KSPS1349YQI							
1	2	3	4	5	6	7	8	9

Protein	Phospho-sites Kinases used	APC/C^{WT} No treatment	APC/C^{WT} Cdk2-cyclinA3	$APC/C^{\Delta Apc3\text{-}loop}$ Cdk2-cyclinA3-Cks2 + Plk1	APC/C^{WT} Cdk2-cyclinA3-Cks2	APC/C^{WT} Plk1	APC/C^{WT} Cdk2-cyclinA3-Cks2 + Plk1	Comparison with published studies Ref.
Apc3	LPNS183CTT							22
	NSCT185TQV							
	SCTT186QVP							
	PNHS192LSH							
	HSLS194HRQ							
	QPET200VLT							
	TVLT203ETP							21
	LTET205PQD							12,21,22
	PQDT209IEL							12
	NLES219SNS	N.D.						22(interphase)
	LESS220NSK	N.D.						21,22
	SSNS222KYS							22
	SKYS225LNT							
	SLNT228DSS							
	NTDS230SVS							
	TSDS231VSY							
	SSVS233YID							
	YIDS237AVI							
	AVIS241PDT							22
	SPDT244VPL							12,22
	GTGT251SIL							
	TGTS252SIL							22
	SILS255KQV							
	KPKT264GRS	N.D.			N.D.			21
	TGRS267LLG				N.D.			
	AALS276PLT							22
	SPLT279PSF							22
	LTPS281PGI							
	PLET289PSP							
	ETPS291PGD						N.D.	12
	QNYT302NTP							12,22
	YTNT304PPV							12,22
	DVPS312TGA							12,22
	VPST313GAP							12,22
	IGQT327GTK	N.D.	N.D.			N.D.		22
	QTGT329KSV							
	GTKS331VFS	N.D.	N.D.			N.D.		
	SVFS334QSG	N.D.				N.D.		21
	FSQS336GNS	N.D.				N.D.		21
	REVT343PIL							12
	LAQT349QSS							
	QTQS351SGP							
	TQSS352GPQ							
	GPQT356STT							
	PQTS357TTP							
	QTST358TPQ							
	TSTT359PQV							
	QVLS364PTI							12
	LSPT366ITS							12,21
	PTIT368SPP							
	TITS369PPN							12,21,22
	RLFT383SDS							21
	LFTS384DSS							21
	TSDS386STT							21
	SDSS387TTK							21
	DSST388TKE							
	SSTT389KEN							21
	GQIT419QPN							
	INDS426LEI							12,21
	LEIT430KLD							12
	KLDS434SII							12
	LDSS435IIS							12,21
	SIIS438EGK							21
	GKIS443TIT							
	KIST444ITP							21,22
	STIT446PQI							12,21
	MNFS761WAM							
	IMGT800DES							
	TDES803QES							
	SQES806SMT							
	QESS807MTD							
	SSMT809DAD							
	ADDT814QLH							
	AAES821DEF							
1	2	3	4	5	6	7	8	9

The pink shading shows the presence of phosphorylation sites and the white indicates its absence.
The phosphorylation sites within the Apc1 AI segment are highlighted in light purple shadows.

Extended Data Table 3 | Summary of phosphorylation sites of *in vitro* phosphorylated APC/C subunits (excluding Apc1 and Apc3) identified by mass spectrometry

Protein	Phospho-sites Kinases used	APC/C^{WT} No treatment	APC/C^{WT} Cdk2-cyclinA3-Cks2 + Plk1	Comparison with published studies Ref.
Apc2	ELDS205RYA			
	LLQS218PLC			21
	RPAS314PEA			12,21,22
	SLETS466GQD			
	GQDS470EDD			22
	EDDS474GEP			
	HQFS532FSP			21
	FSFS534PER			12,21,22
	LIDS732DDE			22(interphase)
	DDES736DSG			22(interphase)
	ESDS738GMA			22(interphase)
	GMAS742QAD			
Apc4	ARVT199GIA			
	KGKY469FNV			12
	DLVS488PPN			
	LDES757SDE			
	DESS758DEE			
	EVLS777ESE			21,22
	LSES779EAE			12
Apc5	PMMT15NGV			21
	HKTS130VVG			
	MELT178SRD			22
	ELTS179RDE			22
	LDVS195VRE			12,21
	QQAS221LLK			21,22
	NDET228KAL			
	KALT232PAS			21
	VASS674AAS			21
Apc6	KDES112GFK			12,22
	NIIS559PPW			12,21,22
	EKQT573AEE			
	AEET577GLT			
	TGLT580PLE			12,21,22
	PLET584SRK			
	LETS585RKT			21,22
	TPDS592RPS		N.D.	
	SRPS595LEE		N.D.	12
	LEET599FEI			12
	MNES607DMM			
	LETS614MSD			
1	2	3	4	5

Protein	Phospho-sites Kinases used	APC/C^{WT} No treatment	APC/C^{WT} Cdk2-cyclinA3-Cks2 + Plk1	Comparison with published studies Ref.
Apc7	VRPS119TGN			12
	RPST120GNS			12
	TGNS123AST			12,22
	NSAS125TPQ			12,22
	SAST126PQS			21,22
	MEGS573GEE			
	LEGS582DSE			
	GSDS584EAA			
Apc8	QGET562PTT			12,21
	TPTT565EVP			12,21
	ANNT582PTR			12,21,22
	NTPT584RRV			12
	RRVS588PLN			21,22
	LNLS593SVT			22
	SSVT596P			21,22
Apc12	VGGS42DGE			
	IGLS51SDP			
	GLSS52DPK			
	DPKS56REQ	N.D.		
	NRSS78QFG			
Apc15	DEDS76EED			
	EEDS80EDD			
	YNES98PDD			
Apc16	SSSS8SAG	N.D.		
	VSGS16SVT	N.D.		
	FSVS26DLA	N.D.		
1	2	3	4	5

The pink shading shows the presence of phosphorylation sites and the white indicates its absence.